Acta Materialia 273 (2024) 119983

Contents lists available at ScienceDirect

Acta Materialia

journal homepage: www.elsevier.com/locate/actamat

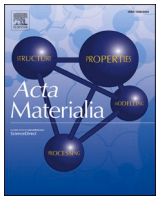

Full length article

Oxygen solutes-regulated low temperature embrittlement and high temperature toughness in vanadium

Pei Wang , Wei-Zhong Han *

Center for Advancing Materials Performance from the Nanoscale, State Key Laboratory for Mechanical Behavior of Materials, Xi'an Jiaotong University, Xi'an 710049, China

ARTICLE INFO

Keywords:
Vanadium
Oxygen
Embrittlement
Toughness
Dislocation

ABSTRACT

The plasticity of body-centered cubic (BCC) metals is sensitive to interstitial trace impurities. Owing to high oxygen affinity, vanadium (V) shows a tendency of embrittlement with increasing oxygen concentration. However, how oxygen solutes affect the ductile-to-brittle transition (DBT) behavior of V remains unclear. In this study, we investigate the DBT behavior of V with different oxygen solute concentrations using small-punch test. As oxygen content increases, the DBT temperature (DBTT) rises incrementally accompanied by a widening of the semi-brittle transition zone. The reduction of the lower fracture energy plateaus indicates a classical low-temperature embrittlement, while the rising of the upper fracture energy plateaus manifests a remarkable high-temperature toughening. Below DBTT, owing to the strong pinning effect of oxygen-vacancy complexes on dislocations, only a limited number of slip systems were activated with very low dislocation density, and all screw dislocations are immobile. Above DBTT, owing to the intensive interactions between dislocation and oxygen-vacancy complexes, frequent dislocation cross-slips trigger multiple slip systems and accelerate dislocation multiplication and storage, all of which contribute to the high-temperature toughness. These findings clarify the effect of oxygen solute on the DBT of V and guide the design of high-performance refractory metals.

1. Introduction

Body-centered cubic (BCC) metals are critical structural materials for extreme service environments, because of their excellent mechanical properties, corrosion resistance and irradiation tolerance [1-3]. However, group VB BCC metals are sensitive to light elements, such as oxygen, carbon and hydrogen, which cause considerable embrittlement tendency and restrict their wide applications [4,5]. Since the 1980s, vanadium (V) alloys have been considered as a potential candidate for blanket material in nuclear fusion reactors owing to their low activation, high-temperature strength, irradiation resistance and good compatibility with liquid lithium [6-13]. However, high oxygen affinity facilitates the absorption of impurities during manufacturing or over long-duration service at 500~750 °C, thwarting its application in nuclear fusion reactors [14,15]. Undesirable oxygen uptaking contributes to prominent hardening and embrittlement, and affects the ductile-to-brittle transition (DBT) behavior of V, entailing a risk of premature fracture [16-22]. Due to different degrees of trace impurity in pure V, the DBT temperature shifts in a wide range of −100 °C to 20 °C [16,23-26]. Therefore, the influence of impurity elements (especially oxygen solutes) on the DBT behavior of V needs to be explored for potential application.

The effect of oxygen solutes on the plasticity of BCC metals has been widely explored. Oxygen solutes usually occupy the octahedral site and cause lattice expansion, which enhances lattice friction and makes dislocations glide difficult, resulting in strengthening with the expense of ductility [27-29]. Because of the unique three-dimensional core structure of screw dislocation in BCC metals, whose motion is thermally activated, thus the interaction between dislocations and oxygen solutes is more complex [30-34]. For example, light elements (C, O, H) solutes tend to segregate in the core of screw dislocations and reconstruct the original dislocation core into a hard-core configuration, which enhances Peierls stresses and the enthalpy for double-kink formation, significantly reducing the dislocation mobility in BCC metals [35-38]. Similarly, the distortion of the dislocation core by oxygen solutes in titanium effectively locks dislocations and renders a "mechanical shuffle" mechanism [39,40].

In addition, oxygen solutes can effectively harden and embrittle BCC metals via the formation of point defect complexes. Oxygen-alloyed BCC high-entropy alloys trap screw dislocations by forming ordered oxygen

* Corresponding author.
E-mail address: wzhanxjtu@mail.xjtu.edu.cn (W.-Z. Han).

https://doi.org/10.1016/j.actamat.2024.119983
Received 14 March 2024; Received in revised form 24 April 2024; Accepted 6 May 2024
Available online 6 May 2024

complexes, which promote double cross-slip and dislocation multiplication [41]. Notably, in oxygen-charged Nb and V, a local repulsive interaction is formed between oxygen atoms and screw dislocations, hence oxygen solutes cannot directly trap screw dislocations [42]. However, owing to strong binding energy between vacancy and oxygen atom, highly stable oxygen-vacancy complexes are produced during plastic deformation. As the number density of oxygen-vacancy complexes increases, the screw dislocations are strongly pinned and cause strengthening or even embrittlement [43,44]. Therefore, the interplay between screw dislocations and oxygen/oxygen-vacancy complexes will affect the DBT behavior of V. Nevertheless, a clear correlation between oxygen solutes and the DBT behavior of V is missing yet. Furthermore, the fundamental mechanisms for oxygen solutes-induced DBT remain intriguing.

In this study, small-punch test (SPT) is used to gauge the DBT behavior of V with different oxygen concentrations. Fracture energies as a function of temperatures mark the DBT of V and show a strong correlation with the oxygen concentration. Based on the upper/lower energy plateaus of SPT, dispersed oxygen solutes not only entail low-temperature embrittlement but also generate anomalous high-temperature toughness. The deformation and fracture characteristics of the V alloys with different oxygen concentrations were explored. The underlying mechanisms for oxygen-regulated DBT behavior in V are further discussed.

2. Experimental methods

2.1. V samples with different oxygen concentration

The hot-rolled polycrystalline V plate (1.0 mm in thickness, 99.95 % purity) was annealed at 1050 °C for 1 h (with a vacuum of $\sim 10^{-4}$ Pa) to obtain a fully recrystallized structures, named as pure V. V sheets with a size of 70 mm (length) × 21 mm (width) × 1 mm (thickness) were used for oxygen-charging in a furnace tube with 20 sccm flowing gas of Ar with 5 % O_2 (about 260 Pa) at the temperature of 800 °C, 900 °C, 1000 °C for 1 h [45]. Three oxygen-charged V samples were further homogenized at 1000 °C for 6 h with a vacuum of $\sim 10^{-4}$ Pa to ensure the uniform distribution of oxygen solutes. The oxygen concentrations are 0.073 at.% for pure V, 0.444 at.% for V charged at 800 °C (named as V-0.5O), 1.012 at.% for V charged at 900 °C (named as V-1.0O) and 1.512 at.% for V charged at 1000 °C (named as V-1.5O) according to an analysis by LECO ONH836 Oxygen Elemental Analyzer. X-ray diffraction (XRD) was utilized to detect the phase structures especially the likely formation of oxides.

2.2. Small-punch test and microstructural characterization

Square-shaped SPT specimens with the size of 7 mm × 7 mm were cut from pure V and three oxygen-charged sheets. The samples were then mechanically ground and electrochemically polished using a solution of 10 % perchloric acid and 90 % glacial acetic acid at 25 V for 90 s at −20 °C. The final thickness of all the SPT samples is 0.500 ± 0.005 mm. The procedure of SPT was described in a previous study [46]. SPT was conducted with a displacement speed of 0.2 mm/min in the temperature range of −100 °C to 240 °C in an environmental chamber. Mechanical loading was stopped after a 20 % load drop from the maximum value. The surface deformation features were examined by HITACHI SU6600 SEM. Dislocation structures were investigated using a JEOL 2100F transmission electron microscope (TEM, 200 KeV) in samples with a controlled SPT displacement of 0.3 mm. TEM foils were mechanically polished to 50 μm followed by twin-jet electropolishing in a solution of 10 % perchloric acid and 90 % alcohol at 50 V and −30 °C. In-situ nanomechanical tests were conducted inside a JEOL 2100F TEM using an electrical tip holder. Real-time videos were recorded by a charge-coupled device camera (CCD, Gatan 833) with 10 frames per second during in-situ compression.

3. Results

3.1. DBT behaviors of V with different oxygen concentration

Fig. 1(a) displays the oxygen-charging procedure, where oxygen gas is decomposed into atoms/ions at the surface of V at high temperature, and subsequently diffuses into the metal matrix during long-time solution treatment at 1000 °C. The initial microstructures of pure V and V-1.5O are displayed in Fig. 1(b). Both samples maintain equiaxed grains with an average size of 50∼150 μm. As shown in Fig. 1(c), the cross-section Vickers hardness of the four samples is uniform, indicating the oxygen solutes distribute homogeneously. The hardness also increases with the oxygen concentration. All samples have a single BCC structure and no obvious oxides, as indicated by the XRD pattern in Fig. 1(d). The left shift of the XRD peaks is owing to the lattice expansion caused by oxygen interstitials [47,48].

Fig. 2(a) shows the temperature-dependent load-displacement curves for four samples with different oxygen concentrations. Pure V exhibits brittleness below 0 °C, with a small peak load of 300 N. The load-displacement curves display several tiny load drops, which correspond to crack nucleation and propagation [49]. In the temperature range of 0 °C to 30 °C, the load rises steadily to a higher peak force followed by abrupt failure, indicating a semi-brittle deformation feature [50-52]. Above 30 °C, pure V shows entirely ductile deformation as manifested by the maximal load on the curves followed by plastic flow [50-52]. V-0.5O, V-1.0O, and V-1.5O all show similar DBT behavior with brittle, semi-brittle and ductile deformation stages, as marked in Fig. 2(a). At lower temperatures, oxygen-charged V shows a direct failure without noticeable plasticity. With the increase in oxygen concentration, the temperature range for the semi-brittle deformation is widened and the DBT temperature also increases. For the ductile deformation stage, the maximum load increases from 600 N for pure V to 1150 N for V-1.5O, which indicates an obvious high-temperature strengthening effect [28,29]. The load-displacement curves of V-1.5O display a sudden load drop after the peak load in the ductile deformation zone, which is related to surface microcracks formation [49,51].

The area underneath the load-displacement curves reflects the SPT fracture energies. Fig. 2(b) plots the fracture energy as a function of temperatures for four types of samples. According to the midpoint of the upper and the lower plateaus of fracture energy, the DBT temperature (DBTT) can be determined, which is 20 °C for pure V, 40 °C for V-0.5O, 65 °C for V-1.0O and 135 °C for V-1.5O. The DBTT of pure V obtained by small-punch test matches well with the previous reports [23-26]. The temperature range for DBT is also widened with the increase in oxygen concentrations. The lower plateau of the fracture energy decreases with the increase of oxygen concentration, as indicated by blue arrows in Fig. 2(b). However, once transformed into the ductile deformation zone, the upper energy plateau of fracture energy rises with the oxygen content, showing an unexpected high-temperature toughening. Fig. 2(c) exhibits the comparison of the maximum load and total displacement of the four samples at the temperatures of −60 °C and 200 °C. The continuous reduction of the SPT displacement causes the decrease in fracture energy plateau at the low-temperature range. In contrast, the less change in the displacement but an obvious increase in the load at high-temperature range cause the high-temperature toughening [23, 24].

3.2. Surface deformation morphologies

Typical fracture morphologies for four samples after SPT are shown in Fig. 3. For pure V, several radial cracks nucleate and gently extend outward below the DBTT (20 °C) (see Fig. 3(a)), corresponding to the flat load-displacement curves in Fig. 2(a). The radial cracks in Fig. 3(u) show brittle fractures with cleavage steps. In contrast, in Figs. 3(b)-(e), the radial cracks transform into annular cracks, which demonstrate a ductile fracture with dimples, as shown in Fig. 3(v). The transition of

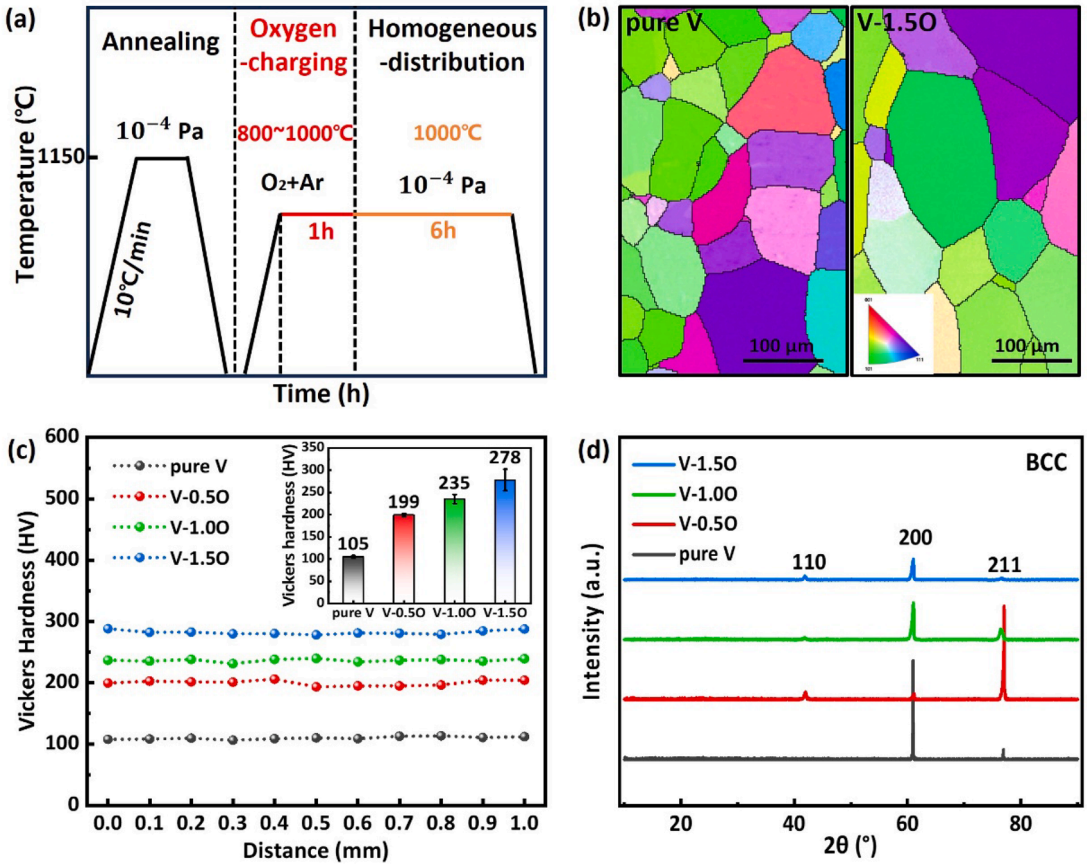

Fig. 1. Samples preparation and initial microstructures. (a) Oxygen-charging procedure for V-O solid solutions. (b) Microstructures of pure V and V-1.5O. (c) Cross-sectional Vickers hardness distribution in pure V and three samples with different oxygen concentration. The insert is the comparison of surface Vickers hardness. (d) X-ray diffraction patterns of pure V and oxygen-charged V.

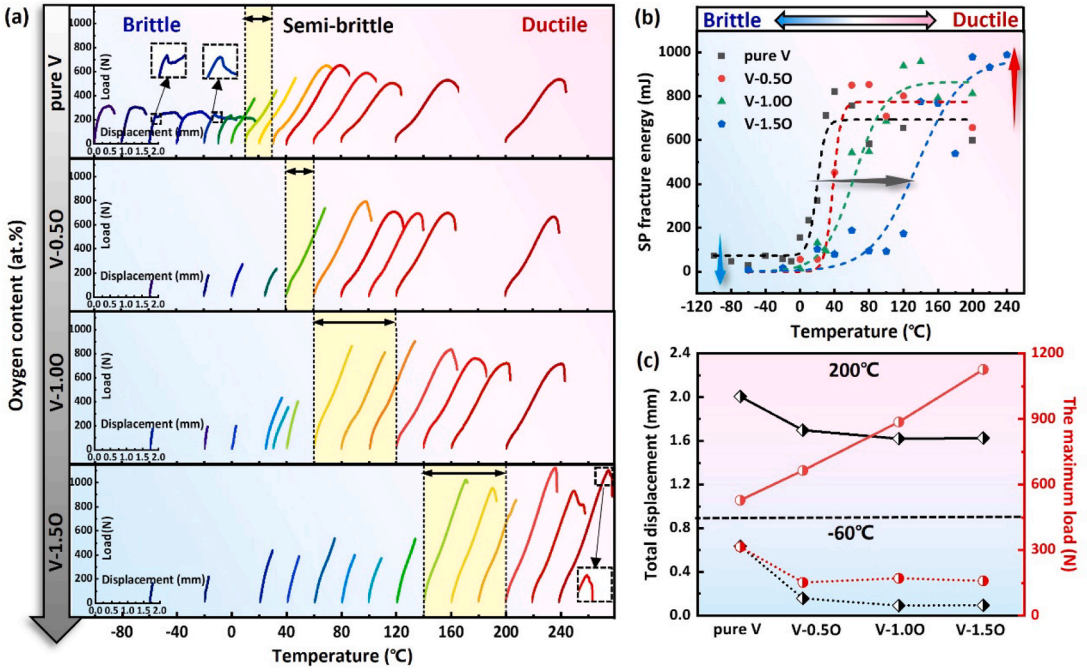

Fig. 2. Small-punch testing of pure V and oxygen-charged V with different oxygen concentration. (a) Load-displacement curves for four types of samples in the temperature range of −100 °C to 240 °C. The arrows in (a) indicate the load drop phenomenon on the curves. (b) Small-punch fracture energies as a function of temperatures. The shift of DBTT and the change of upper/lower energy plateau with the increasing oxygen concentration are indicated by arrows. (c) Comparison of total displacement and the maximum load of four samples at testing temperature of −60 °C and 200 °C.

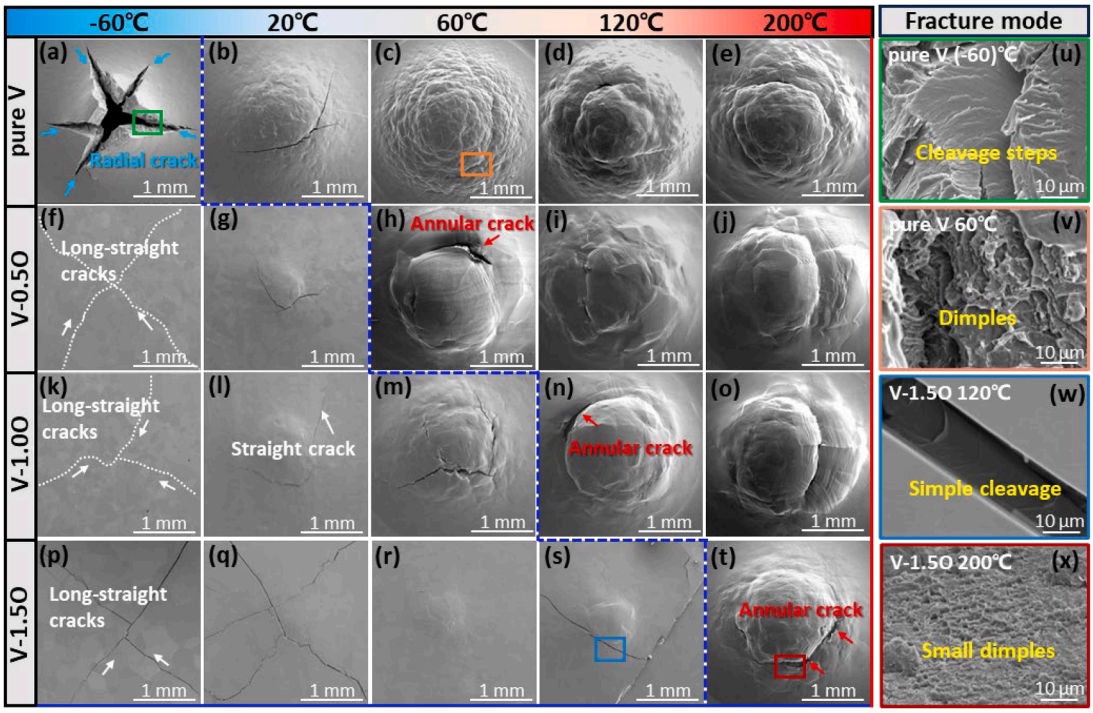

Fig. 3. Temperature-dependent surface fracture morphologies of pure V and three oxygen- charged V samples after small-punch testing. (a-e) pure V; (f-j) V-0.5O; (k-o) V-1.0O; (p-t) V-1.5O. (u-x) Enlarged SEM images of the area marked in (a), (c), (s) and (t) showing different fracture characteristics.

crack extension mode indicates the DBT of pure V and is consistent with the load-displacement curves [46]. With the addition of oxygen solutes, fracture morphologies evolve for three types of oxygen-charged samples, as shown in Fig. 3(f)-(t). In Figs. 3(f), (k) and (p)-(s), long-straight cracks rapidly propagate without macroscopic plastic deformation below the DBTT, as highlighted in Fig. 3(w). Oxygen impurities immediately reduce the resistance to crack extension compared to pure V, manifesting a low-temperature embrittlement. The transition temperature from radial cracks to annular cracks continues to increase with the oxygen concentration, as separated by the dotted line in Fig. 3. Above the DBTT, typical annular crack expands slowly in Figs. 3(h), (n) and (t), which dominates the high-temperature deformation. Meanwhile, the

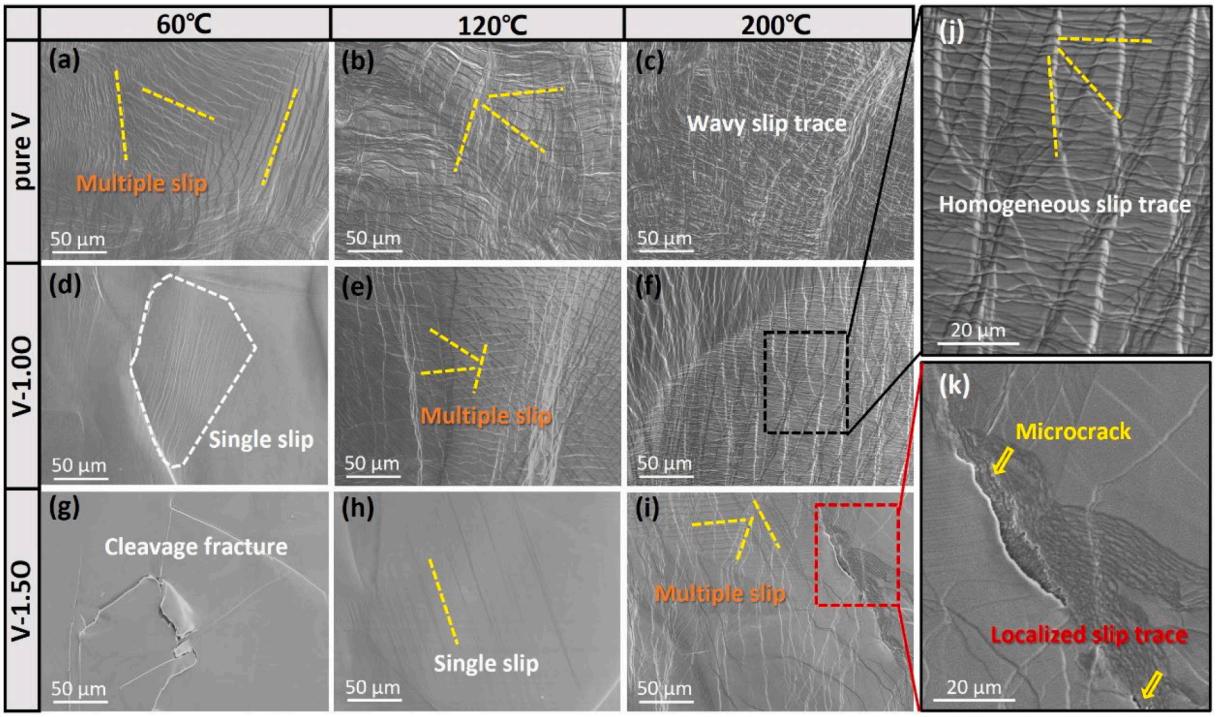

Fig. 4. Surface deformation features of pure V, V-1.0O and V-1.5O after small-punch testing. (a-c) Wavy slip trace of pure V. (d-f) Long-straight slip trace of V-1.0O. (g-i) Inhomogeneous slip trace of V-1.5O. (j) Enlarged images of the area marked in (f) with high density of homogeneous slip trace. (k) Enlarged images of the area marked in (i) showing localized slip trace with microcracks.

V-1.5O sample punched at 200 °C displays denser and much smaller dimples on the fracture surface compared to that of pure V, as shown in Fig. 3(x).

The DBT behavior can also be reflected by the distinctive surface slip features, as shown in Fig. 4. In general, only a single slip system is activated below the DBTT, and multiple slips are operated above the DBTT [53]. For pure V, the density of slip traces increases with temperature above the DBTT (20 °C), as shown in Fig. 4(a)-(c). V-1.0O shows a clear single slip in some grains below the DBTT (40 °C), while uniformly distributed multi-slip traces are visible at elevated temperatures, as shown in Fig. 4(d)-(f). The long-straight slip traces become denser and more homogeneous for V-1.0O (Fig. 4(j)), indicating a high-temperature toughness. For V-1.5O, the multiple slip traces formed above the DBTT show a peculiar inhomogeneous distribution, as highlighted in Fig. 4(i) and (k). Localized slip bands accompanied by the formation of microcracks explain the small load drops in the load-displacement curves in Fig. 3(a).

3.3. Oxygen-mediated dislocation structural evolution

Fig. 5 shows the dislocation structures in pure V after brittle and ductile deformation, all the TEM images are taken under different two-beam conditions, as indicated in the figure. For pure V, after brittle deformation (0 °C), the dislocations are short and straight, which are primarily screw dislocations. After ductile deformation (40 °C), a high density of entangled dislocations on three {110}⟨111⟩ slip systems ensure good deformability. Heavily entangled mixed dislocations with a large number of dislocation junctions and dislocation loops are formed, manifesting frequent dislocation-dislocation interactions in the ductile deformation regime [54].

For V-1.0O, after brittle deformation, three slip systems are launched with low density of long-straight screw dislocations, and a few short parallel edge segments, as shown in Fig. 6(a)-(d). There are many kinks and local bowing-out features on the screw dislocations along with some ring-like dislocation debris. The limited curvature in the bowing region implies that the screw dislocations are pinned because of high oxygen concentration. After punching at 120 °C, the dislocation density significantly increased, massive long-straight screw dislocations and entangled mixed segments with a homogeneous distribution are arranged along multiple {110} slip planes, as shown in Fig. 6(e)-(k). As highlighted in Fig. 6(h)-(j), long-straight screw dislocations show zigzag features due to a large number of consecutive pinning points, and leave a high density of dislocation debris [30,31,44], which are beneficial for the high-temperature strength, as shown in Fig. 2(a). In addition, the majority of screw dislocations have a curved bowing-out geometry, as shown in Fig. 6(i).

Compared with pure V and V-1.0O, the dislocation density is relatively low in V-1.5O, as shown in Fig. 7. Screw dislocations disappear after low temperatures punching in the V-1.5O sample, leaving only partial edge dislocation segments (Fig. 7(a) to (c)), which is uncommon in BCC metals [31,55]. Because of the high oxygen concentration, the mobility of screw dislocations is entirely lost, and even the mobility of edge dislocations is also significantly reduced and remained in the microstructure after punching. These nearly immobile low-density dislocations are unable to blunt crack tips [53]. Consequently, the V-1.5O sample fails by rapid expansion of long-straight cracks without noticeable plastic deformation below the DBTT, as shown in Fig. 3(w). Above the DBTT (135 °C), intense long-straight dislocations and curved mix-dislocation segments are oriented along two slip planes, as shown in Fig. 7(e)-(k). These dislocations show a peculiar non-uniform distribution characteristic in a wide region. The representative regions A and B on both sides of a low-angle grain boundary (LAGB) have totally different dislocation structures, as shown in Fig. 7(e) and (f). Region A contains localized aggregation zones with dense slip bands, whereas Region B displays sporadically arranged low-density dislocations. The inhomogeneous deformation and heterogeneous distribution of dislocations are typical features in various V-1.5O samples. The dense slip band formed in V-1.5O is characterized in detail in Fig. 7(h)-(k), which is composed of tightly packed long-straight screw dislocations and mixed segments with a bowing out geometry on multiple slip planes. In this region, a high level of dislocation debris is also produced within the localized deformation band. Such specialized dislocation configuration is likely caused by the interaction of dislocations and localized obstacles, which could provide strong back stress hardening [56]. Nevertheless, the localized concentration of dislocations induces stress concentration and causes microcrack nucleation near the localized slip traces, as shown in Fig. 4(k).

3.4. Dynamic interplay between dislocation and oxygen solutes

The influence of oxygen impurities on the dynamic behaviors of dislocations was investigated by in-situ nanomechanical tests on pure V

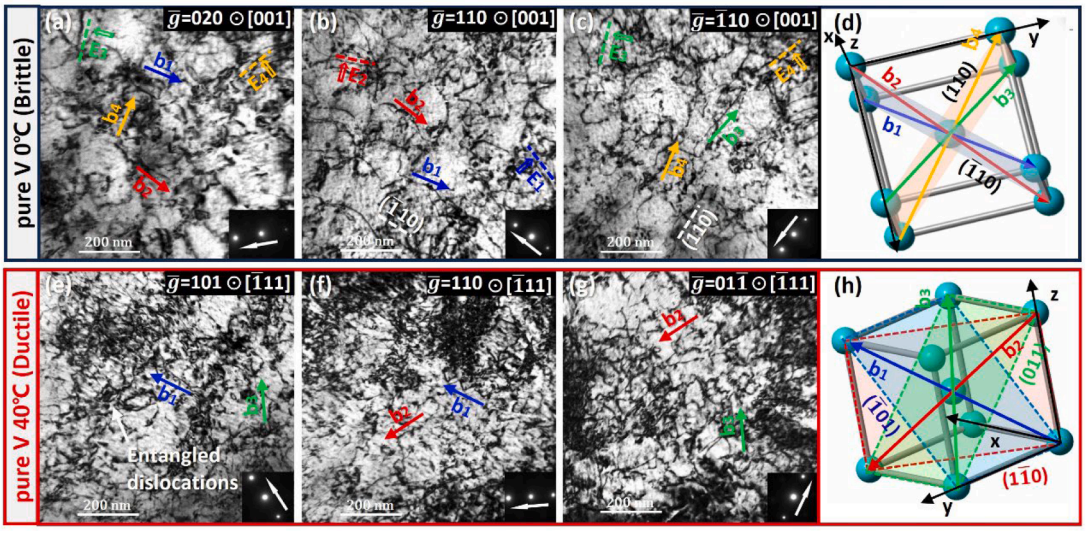

Fig. 5. Dislocation structures in pure V after punching to a displacement of 0.3 mm at 0 °C (below DBTT) and 40 °C (above DBTT). (a-d) Slightly curved dislocations formed on (110) and (1̄10) planes in pure V after brittle deformation. (e-h) High density entangled dislocations formed on three {110} ⟨111⟩ slip systems after ductile deformation. The $\vec{b}_1$, $\vec{b}_2$, $\vec{b}_3$ and $\vec{b}_4$ are Burgers vectors of 1/2[111], 1/2[11$\bar{1}$], 1/2[$\bar{1}$1$\bar{1}$] and 1/2[$\bar{1}$11].

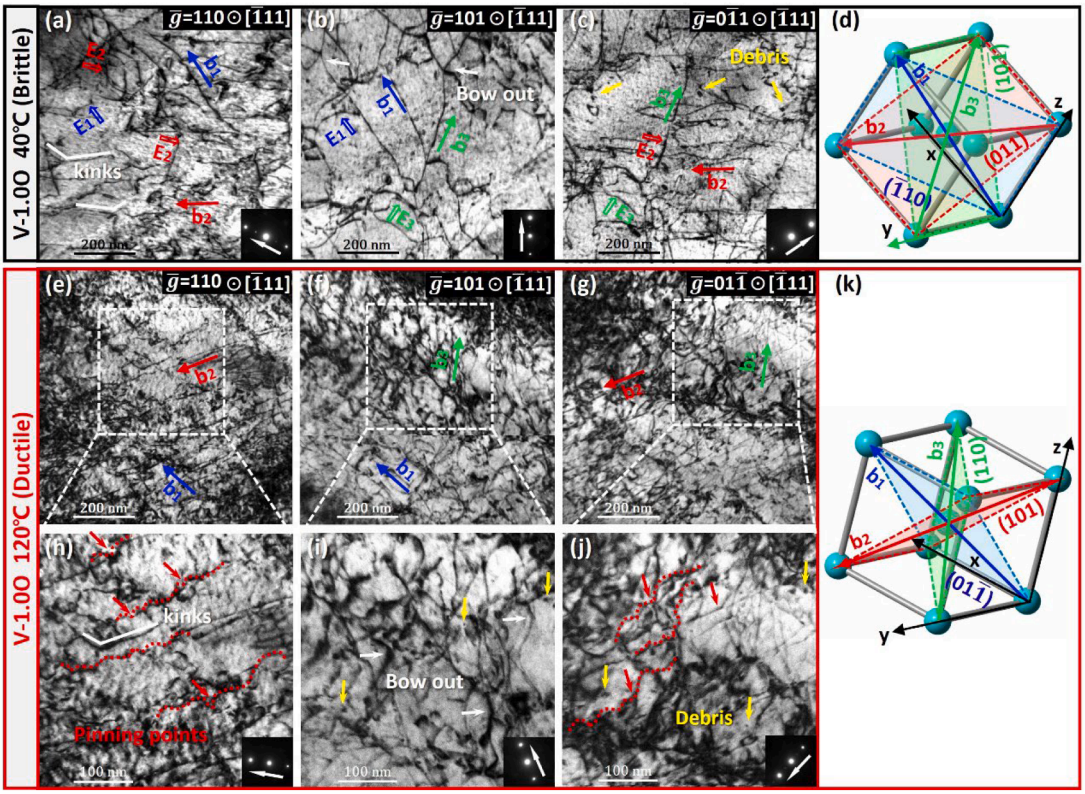

Fig. 6. Dislocation structures in V-1.0O after punching to a displacement of 0.3 mm at 40 °C (a-d) and 120 °C (e-k). (a-d) Low density of long-straight dislocations along three slip planes after brittle deformation, "E" marks the edge dislocation segments. (e-k) Massive dislocations well-arranged along multiple {110} slip planes after ductile deformation. (h)-(j) Highlight of the dislocation structures in (e-g).

and V-1.5O samples, as shown in Fig. 8 and Movies S1 to S2. Bundles of dislocations along two $[\bar{1}1\bar{1}]$ and $[11\bar{1}]$ directions successively nucleate and smoothly glide forward when the tip of the indenter touches the pure V thin foil, as shown in Movie S1 and the static screenshots in Fig. 8 (a). The coloring curved lines show the trace of dislocations d_1 and d_2, which are mixed dislocations consisting of parallel long-straight screw dislocation segments and a vertical edge dislocation segment. Dislocation d_1 and d_2 slip forward during compression with a screw/edge dislocation velocity ratio of 0.64 and 0.75 at room temperature. Both screw and edge segments of dislocation move forward cooperatively with a high velocity and continue to form high-density and closely compacted dislocation groups, which form efficient dislocation sources to ensure the excellent room-temperature deformability of pure V [44].

In contrast, the V-1.5O sample displays entirely different dislocation dynamic characteristics, as shown in Fig. 8(b). During the repeated loading-unloading process, neither nascent dislocation nucleation nor the pre-exist dislocations gliding are captured. The pre-existing dislocations are all pinned. As shown in Movie S2, the thin foil of V-1.5O recovers elastically during the unloading process, with no plastic deformation because of the immobile dislocations during the compression procedure. These observations demonstrate a strong pinning effect generated by the 1.5 at.% oxygen solutes. The initial dislocations are completely locked and lose their mobility, resulting in a rapid deficiency of the ability to accommodate plastic deformation and arrest the crack propagation, as manifested by the brittle fracture at room temperature in V-1.5O (see Fig. 3).

4. Discussion

4.1. Oxygen solutes induced low-temperature embrittlement

Oxygen solutes seriously embrittle V at low temperatures, as manifested by a reduction in the lower fracture energy plateau and a dramatic decrease in the deformation ability. As shown in Fig. 3, the transition from slowly propagating cracks in pure V to long-straight and rapidly expanding cracks in oxygen-charged V is related to the dynamics of dislocations [46,57,58]. Fig. 9(a) displays the variation of dislocation density with the oxygen concentration. Bellow the DBTT, the dislocation density drops from 4.73×10^{-4} m^{-2} in pure V to 1.33×10^{-4} m^{-2} in V-1.5O, as indicated by the blue arrow in Fig. 9(a). As shown in Fig. 9(b), curved mixed dislocations are the main microstructural features in pure V after brittle deformation, while the fraction of long-straight screw dislocations increases in V-1.0O below DBTT. Notably, only sparsely distributed short-straight edge segments are observed in V-1.5O other than long-straight screw dislocations [30,31]. This phenomenon is related to the locking effect of oxygen solutes on both screw and edge dislocations below DBTT.

An earlier study reported that there is a repulsive interaction between oxygen solutes and screw dislocations, while oppositely an attractive force between oxygen solutes and edge dislocations [42]. Hence, the oxygen solutes can directly lock edge dislocations but cannot trap the screw dislocations [42]. According to first-principles calculations, oxygen solute and vacancy have a high binding energy of −0.8 eV and tend to form into oxygen-vacancy (O-V) complexes in Nb, which effectively trap screw dislocations because of their attraction [42-44]. Similarly, oxygen solute and vacancy also have a binding energy of −0.42 to −0.8 eV in V, which facilitates the formation of the O-V complexes, containing a vacancy and two oxygen atoms to form a stable spindle-like structure according to first-principles calculations [59-61]. The O-V complexes in V can obstruct the motion of screw dislocations at low temperatures, because of the superior binding energy between O-V complexes and the screw dislocations [42]. Therefore, all screw dislocations lost their mobility because of the high oxygen concentration (see Movie S2). However, an attractive force between oxygen solutes and

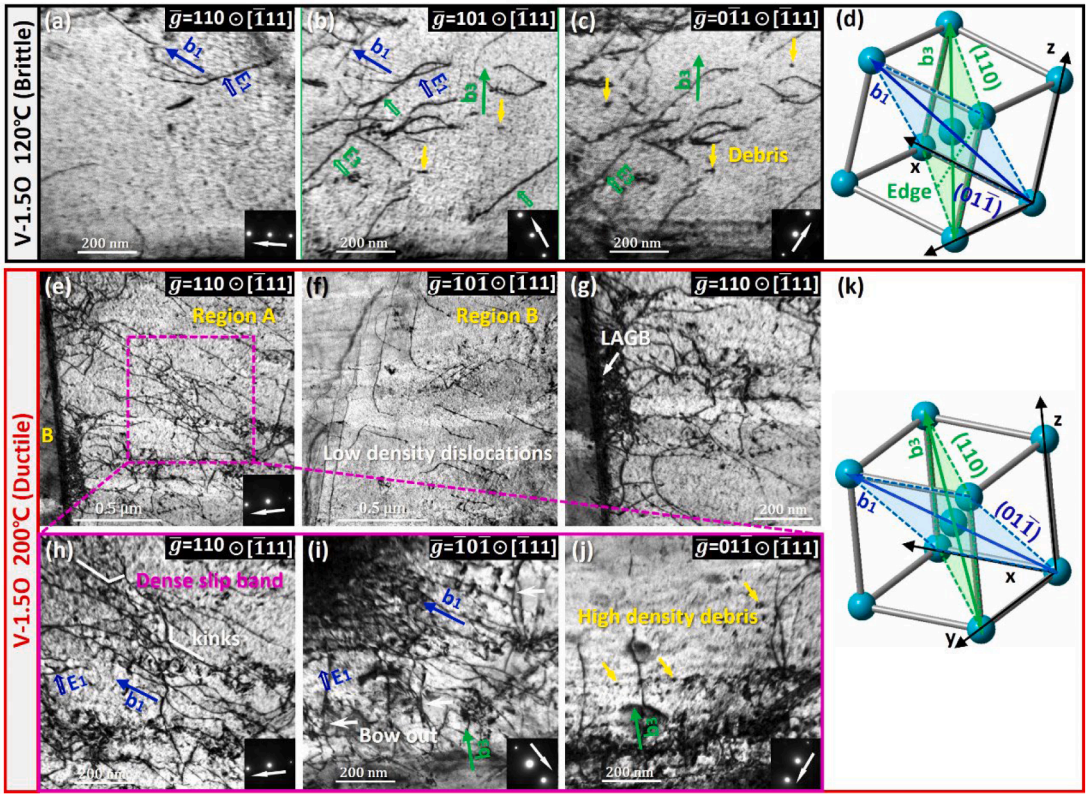

Fig. 7. Dislocation structures in V-1.5O after punching to a displacement of 0.3 mm at 120 °C (a-d) and 200 °C (e-k). (a-d) Parallel arranged sparse edge dislocations on (110) and (01$\bar{1}$) planes after brittle deformation. (e-k) Profuse dislocation structures on both sides of the grain boundary with non-uniform distribution after ductile deformation. (e) Region A highlights a dense slip band. (f) Region B shows an area with low-density dislocations. (g) Dislocations around the grain boundary. (h)-(j) Highlight dense slip band in (e) with intense long-straight screw dislocations on (110) and (01$\bar{1}$) planes and large amounts of debris.

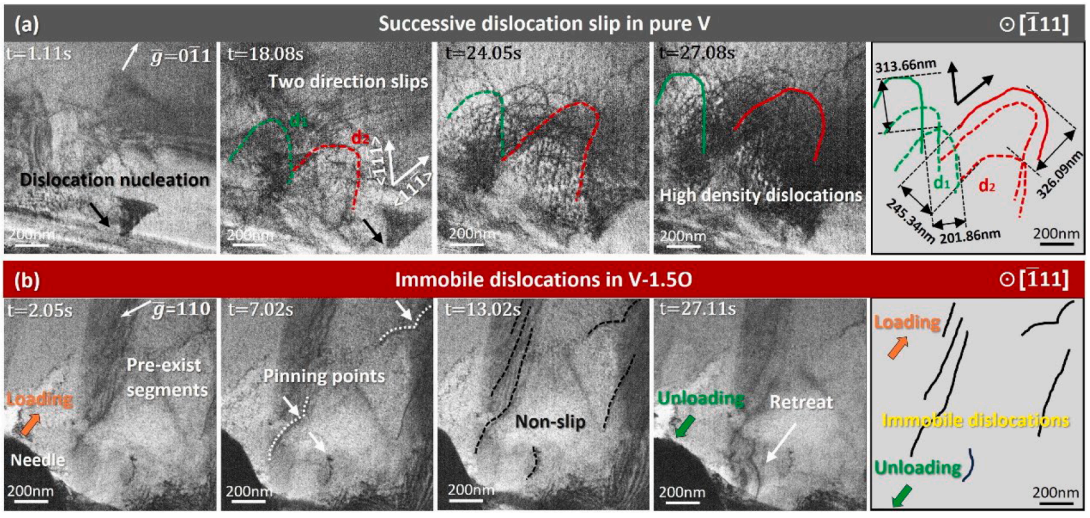

Fig. 8. In-situ nanomechanical tests showing the gliding of dislocations in pure V and V-1.5O samples at RT. (a) Nucleation and gliding of dislocations in pure V thin foil during compression. Two dislocations marked with d_1 and d_2 are highlighted in cartoon. (b) Some immobile dislocations are observed in VO-1.5 during in-situ compression at RT.

edge dislocations makes the oxygen solutes can directly pin edge dislocations as well, and only a small fraction of mobile edge dislocations involved in the plasticity of V-1.5O remained in the microstructures after brittle deformation [42].

As summarized in Fig. 10(a)-(c), with the increasing oxygen concentration, dislocation structures evolve from mixed dislocations in pure V to long-straight screw dislocations in V-1.0O, and finally only pure edge dislocations in V-1.5O below DBTT. The evolution of dislocation structures is caused by the pinning effect of O-V complexes on both screw and edge dislocations. The formation of high-density O-V complexes in oxygen-charged V heavily impedes the movement of screw dislocations first, which can also trap edge dislocations at high concentrations, thereby gradually reducing the ability of dislocation multiplications [46,53]. Therefore, a shortage of mobile dislocations during

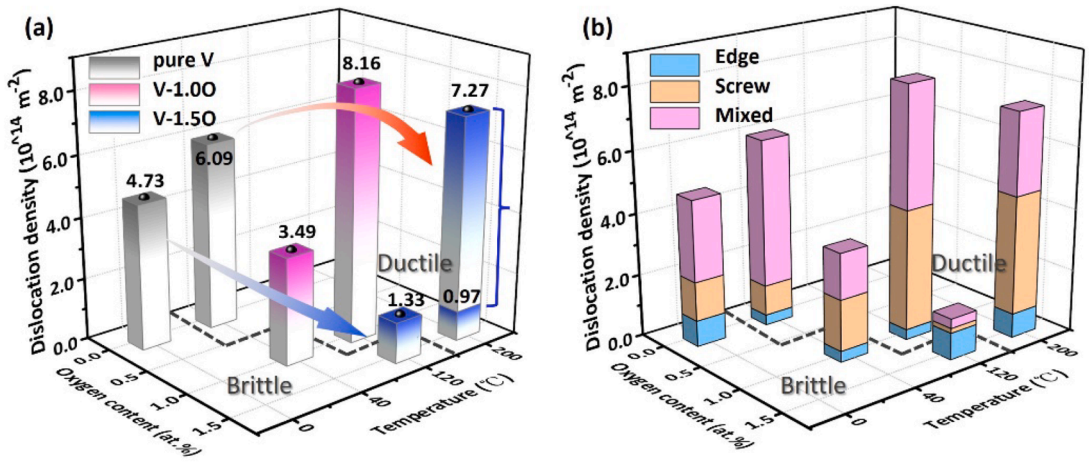

Fig. 9. Statistics of dislocation structures in pure V and oxygen charged V after controlled SPT. (a) Evolution of dislocation density in V with different oxygen concentrations at different testing temperatures according to TEM observations. The blue and red arrows mark the variation of dislocation density for brittle and ductile test conditions. (b) The fraction of edge, screw and mixed dislocation in (a) for different samples and testing conditions.

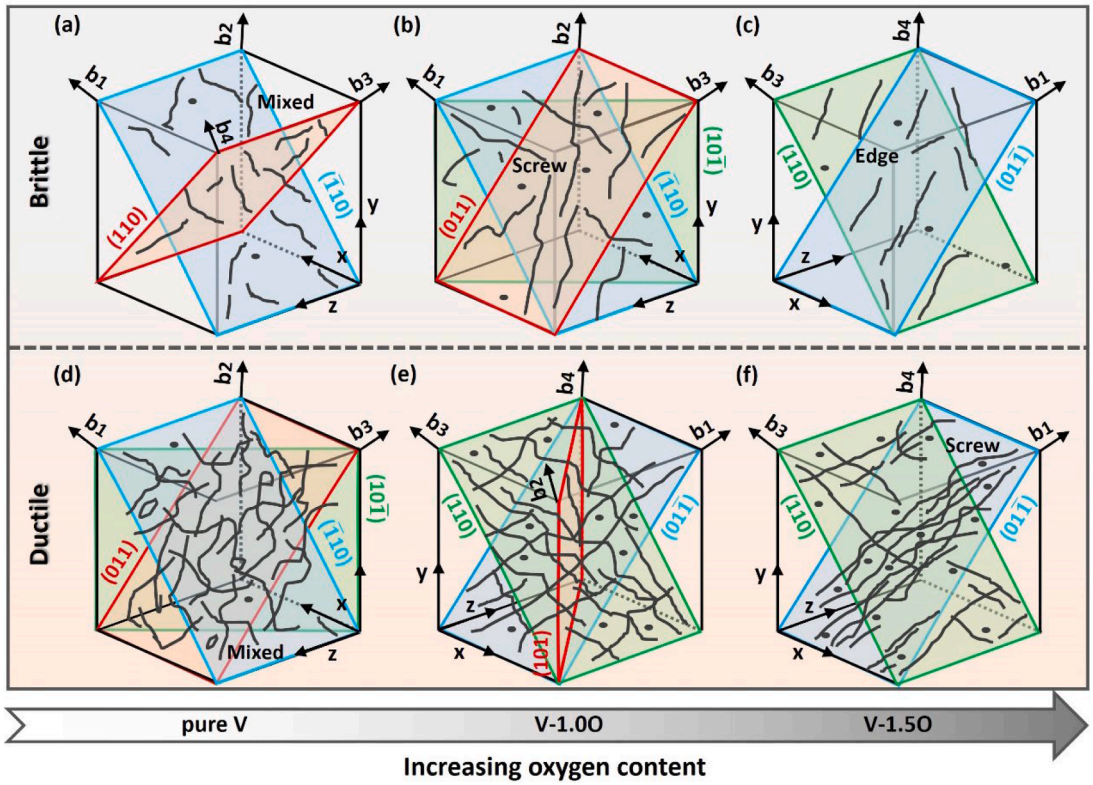

Fig. 10. Schematic diagrams of dislocation structures in pure V, V-1.0O and V-1.5O. (a-c) Decreasing of dislocation density and transition from curved mixed dislocations to edge segments with the increasing of oxygen concentration after brittle deformation. (d-f) Dislocations transition from high-density entangled morphology to long-straight homogenous distribution and then to inhomogeneous distribution with the increasing of oxygen concentration after ductile deformation.

loading is the origin of the low-temperature embrittlement in oxygen-charged V [46-48,58].

4.2. *Oxygen solutes regulated high-temperature toughness*

Oxygen solutes induce a significant high-temperature toughening effect in V, as shown in Fig. 2. For the V-1.0O sample, the dislocation density after ductile deformation reaches a higher level than that of pure V, from 6.09×10^{-4} m^{-2} to 8.16×10^{-4} m^{-2}, and contains a larger fraction of screw dislocations, as displayed in Fig. 9. High density of long-straight screw dislocations and curved mixed dislocations dominate the high-temperature deformation (see in Fig. 6(e)-(k)). Due to the pinning effect of O-V complexes, frequent dislocation cross-slips are promoted above DBTT [40,41]. Although the atomic-sized O-V complexes are not visible under conventional TEM, abundant loop-shaped debris is left after the dislocations bypass them [42-44]. This is similar to the Orowan loops produced by the dislocation-precipitate interactions [62]. Large amounts of dislocation debris are a direct indication of the interaction between dislocations and O-V complexes. The O-V complexes are very stable even in strained samples [43,60,61], thus, the dispersed O-V complexes provide a continuous pinning effect on dislocation lines, which assist dislocation multiplications and storage by

triggering the multiple slip systems, and lead to significant high-temperature strengthening effect, as illustrated in Fig. 10(e).

In contrast to V-1.0O, a unique inhomogeneous dislocation structure is formed in V-1.5O after the high-temperature deformation. The dislocation structures can be divided into two regions, localized dense slip bands with a high dislocation density of 7.27×10^{-4} m^{-2} and homogenous deformation regions with a low dislocation density of 0.97×10^{-4} m^{-2} (see Fig. 9). As indicated by the red arrows in Fig. 9(a), the total dislocation density in V-1.5O after ductile deformation only slightly decreases, but the dense slip bands still maintain a very high dislocation density. Intensive dislocation debris is dispersed in the localized slip zones, which implies that the O-V complexes are inhomogeneously distributed in V-1.5O [42-44]. Heat-activated vacancies during high-temperature annealing are prone to be stabilized by oxygen solutes and then polymerize into short-range ordered complexes V-O_n [60,61]. The dense slip bands are formed in regions with lower levels of O-V complexes, and result in the inhomogeneous dislocation structure [40,42].

As summarized in Fig. 10(f), the dislocations still have good gliding ability in V-1.5O above DBTT. On the one hand, the screw dislocations are locked down and gradually aggregated to form localized dense slip bands in regions with low levels of O-V complexes [41,54,56]. With the accumulation of local stresses, some dislocations bypass the obstacles via the formation of kinks or double cross-slips, thus stimulating multiple slip systems [39,44]. On the other hand, aggregated regions of O-V complexes severely impede dislocations and contribute to the formation of sparse dislocation regions. The dense slip bands as reinforced zones to bear the greater plastic strain, while the low dislocation density regions share more load [63]. Although some surface microcracks are nucleated due to strain localization (Fig. 4), the mobile dislocations could effectively blunt crack propagation at high temperatures, and thus withstand the integrity of the sample above DBTT [53,57]. Therefore, the V-1.5O holds the maximum load successfully at high temperatures while forming inhomogeneous dislocation structures.

4.3. Origin of oxygen-dependent DBT in V

The DBT behavior of BCC metals is controlled by the relative velocity of screw dislocation versus edge dislocation [64,65]. Below the DBTT, screw dislocation has much smaller mobility than edge dislocation, which leads to low dislocation source efficiency and causes brittleness [64]. Above the DBTT, the mobility of screw and edge dislocations are comparable, enabling coordinated motion and generating numerous mobile dislocations to sustain ductile deformation [64,65]. With the increasing of oxygen concentration, the density of O-V complexes increases quickly and gradually evolves from evenly dispersed complexes to an inhomogeneous distribution of short-range ordered complexes [60,61]. Screw dislocations are severely trapped by the scattered O-V complexes, and the ratio of mobility of screw dislocations to edge dislocations is reduced or even approaches zero, and finally lost the ability to generate mobile dislocations, resulting in low-temperature embrittlement. Once reaching a critical temperature, the local thermal activation assists screw dislocations escaping from the O-V complexes and bypassing the obstacles. The mobility of screw dislocations gradually increases and becomes comparable with edge dislocations, ensuring the formation of efficient Frank-Read sources to promote dislocation multiplication and contribute to excellent deformability [41,64]. With a high density of O-V complexes, a higher temperature is required to ensure the easy gliding of screw dislocations, bringing an obvious increase in the DBTT. During loading, dislocations go through a repetitive locking-unlocking process during the semi-brittle zone, which widens the semi-brittle zones in Fig. 2 [58]. V with high oxygen concentration exhibits superb high-temperature toughness because of the dynamic interaction between dislocations and O-V complexes, which facilitate efficient dislocations multiplications and storage above DBTT.

5. Conclusions

In this study, we systematically investigated the oxygen solutes regulated DBT behavior of V and its underlying mechanisms. The main findings are listed below:

(1) With the increasing of oxygen concentration, the DBTT of V rises incrementally accompanied by a widening of the semi-brittle transition zone. At low temperatures, oxygen solutes induce classical brittleness as rapidly expanding long-straight cracks. At high temperatures, tremendous toughness is realized, facilitated by significant strengthening and lossless plasticity.
(2) Bellow DBTT, O-V complexes reduce the slip systems and drop the dislocation density by pinning screw dislocations and freezing their motion, causing low-temperature embrittlement. As the temperature increases, part of dislocations escape from O-V complexes by the formation of kinks and double cross-slips with the assistance of thermal activation. Dislocations repeatedly undergo a locking-unlocking process and make the bulk sample showing a wider semi-brittle zone.
(3) Above DBTT, because of the interactions between dislocations and O-V complexes, an excellent balance with strength and ductility is achieved. The pinning effects of intensive complexes contribute to a significant strengthening and storage of dislocations. Frequent dislocation cross-slips accelerate dislocation multiplication and trigger extensive multiple slip systems, inducing a homogeneous plasticity. Both of which contribute to a considerable high-temperature toughness.

CRediT authorship contribution statement

Pei Wang: Investigation, Methodology, Validation, Writing – original draft. **Wei-Zhong Han:** Conceptualization, Investigation, Methodology, Project administration, Resources, Supervision, Validation, Writing – original draft, Writing – review & editing.

Declaration of competing interest

The authors declare that they have no known competing financial interests or personal relationships that could have appeared to influence the work reported in this paper.

Acknowledgements

This research was supported by the National Natural Science Foundation of China (Grants No 51971170 and 51922082), and the Shaanxi Science & Technology Innovation Project (Grant No. 2022QFY10–03).

Supplementary materials

Supplementary material associated with this article can be found, in the online version, at doi:10.1016/j.actamat.2024.119983.

References

[1] A.A. Johnson, The ductile-brittle transition in body-centred cubic transition metals, Philos. Mag. 7 (1962) 177–196.
[2] M.S. El-Genk, J.M. Tournier, A review of refractory metal alloys and mechanically alloyed-oxide dispersion strengthened steels for space nuclear power systems, J. Nucl. Mater. 340 (2005) 93–112.
[3] J. Knaster, A. Moeslang, T. Muroga, Materials research for fusion, Nat. Phys. 12 (5) (2016) 424–434.
[4] J.R. Donoso, R.E. Reed-Hill, Slow strain-rate embrittlement of niobium by Oxygen, Metall. Trans. A 7A (1976) 961–965.
[5] B.A. Pint, J.R. DiStefano, The role of oxygen uptake and scale formation on the embrittlement of vanadium alloys, Oxid. Metals 63 (2005) 33–55.
[6] D.L. Smith, B.A. Loomis, D.R. Diercks, Vanadium-base alloys for fusion reactor applications-a review, J. Nucl. Mater. 135 (1985) 125–139.

[7] R.F. Mattas, B.A. Loomis, D.L. Smith, Vanadium alloys for fusion reactor applications, JOM 44 (1992) 26–29.
[8] H.M. Chung, B.A. Loomis, D.L. Smith, Properties of vanadium-base alloys irradiated in the Dynamic Helium Charging Experiment, J. Nucl. Mater. 233-237 (1996) 466–475.
[9] D.L. Smith, M.C. Billone, K. Natesan, Vanadium-base alloys for fusion first-wall/blanket applications, Int. J. Refract. Metals Hard Mater. 18 (2000) 213–224.
[10] L. Man, S.L. Yang, The application and development of vanadium in the fields of catalysts and materials, Adv. Mater. Res. 396-398 (2011) 267–273.
[11] H.Y. Fu, J.M. Chen, P.F. Zheng, T. Nagasaka, T. Muroga, Z.D. Li, S. Cui, Z.Y. Xu, Fabrication using electron beam melting of a V-4Cr-4Ti alloy and its thermo-mechanical strengthening study, J. Nucl. Mater. 442 (2013) S336–S340.
[12] T. Muroga, J.M. Chen, V.M. Chernov, R.J. Kurtz, M.Le Flem, Present status of vanadium alloys for fusion applications, J. Nucl. Mater. 455 (2014) 263–268.
[13] T. Nagasaka, T. Muroga, Vanadium for Nuclear Systems, Compr. Nucl. Mater. 6 (2020) 1–18.
[14] R.C. Svedberg, R.W. Buckman, Gas-metal reactions in vanadium and vanadium-base alloys, Int. Metals Rev. 25 (1980) 223–231.
[15] K. Natesan, W.K. Soppet, M. Uz, Effects of oxygen and oxidation on tensile behavior of V-4Cr-4Ti alloy, J. Nucl. Mater. 258-263 (1998) 1476–1481.
[16] O.N. Carlson, D.G. Alexander, G. Elssner, The effect of oxygen on the strength and ductility of polycrystalline vanadium in the range of 4.2 to 400 K, Metall. Trans. A 8 (1977) 99–104.
[17] J.R. DiStefano, J.H. DeVan, Reactions of oxygen with V-Cr-Ti alloys, J. Nucl. Mater. 249 (1997) 150–158.
[18] J.R. DiStefano, B.A. Pint, J.H. DeVan, H.D. Rohrig, L.D. Chitwood, Effects of oxygen and hydrogen at low pressure on the mechanical properties of V-Cr-Ti alloys, J. Nucl. Mater. 283-287 (2000) 841–845.
[19] J.M. Chen, S.Y. Qiu, L. Yang, Z.Y. Xu, Y. Deng, Y. Xu, Effects of oxygen, hydrogen and neutron irradiation on the mechanical properties of several vanadium alloys, J. Nucl. Mater. 302 (2002) 135–142.
[20] I.A. Ditenberg, I.V. Smirnov, K.V. Grinyaev, A.N. Tyumentsev, V.M. Chernov, M. M. Potapenko, Influence of oxygen concentration on mechanical properties and fracture features of V-Me (Cr, W)-Zr-system vanadium alloys at different temperatures, Mater. Sci. Eng. A 874 (2023) 145041.
[21] P. Gumbsch, J. Riedle, A. Hartmaier, H.F. Fischmeister, Controlling factors for the brittle-to-ductile transition in tungsten single crystals, Science 282 (1998) 1293–1295.
[22] M. Tanaka, E. Tarleton, S.G. Roberts, The brittle-ductile transition in single-crystal iron, Acta Mater 56 (2008) 5123–5129.
[23] J.A. Rinebolt, W.J. Harris, Effect of carbon content on the energy-transition-temperature curves for steel, Trans. Am. Soc. Met. 43 (1951) 1197.
[24] W.A. Spitzig, The effects of phosphorus on the mechanical properties of low-carbon iron, Metall. Trans. 3 (5) (1972) 1183–1188.
[25] D.L. Smith, H.M. Chung, H. Matsui, A.F. Rowcliffe, Progress in vanadium alloy development for fusion application, Fusion Eng. Des. 41 (1998) 7–14.
[26] T.D. Joseph, M. Tanaka, A.J. Wilkinson, S.G. Roberts, Brittle-ductile transitions in vanadium and iron-chromium, J. Nucl. Mater. 367-370 (2007) 637–643.
[27] R.H. Li, P.B. Zhang, X.Q. Li, C. Zhang, J.J. Zhao, First-principles study of the behavior of O, N and C impurities in vanadium solids, J. Nucl. Mater. 435 (2013) 71–76.
[28] M.G. Jo, P.P. Madakashira, J.Y. Suh, H.N. Han, Effect of oxygen and nitrogen on microstructure and mechanical properties of vanadium, Mater. Sci. Eng. A 675 (2016) 92–98.
[29] T. Kainuma, N. Iwao, T. Suzuki, R. Watanabe, Effects of oxygen, nitrogen and carbon additions on the mechanical properties of vanadium and V/Mo alloys, J. Nucl. Mater. 80 (1979) 339–347.
[30] Y. Huang, R.J. Arsenault, The Effect of oxygen on the dislocation structures in vanadium, Mater. Sci. Eng. 12 (1973) 111–118.
[31] J.W. Christian, Some surprising features of the plastic deformation of Body-Centered Cubic metals and alloys, Metall. Mater. Trans. A 14 (7) (1983) 1237–1256.
[32] M.S. Duesbery, V. Vitek, Plastic anisotropy in bcc transition metals, Acta Mater 46 (5) (1998) 1481–1492.
[33] J. Marian, W. Cai, V.V. Bulatov, Dynamic transitions from smooth to rough to twinning in dislocation motion, Nat. Mater. 3 (3) (2004) 158–163.
[34] V. Vitek, V. Paidar, Non-planar dislocation cores: a ubiquitous phenomenon affecting mechanical properties of crystalline materials, in: J.P. Hirth (Ed.), Dislocations in Solids, Elsevier, Amsterdam, 2008, pp. 439–514.
[35] L. Ventelon, B. Luthi, E. Clouet, L. Proville, B. Legrand, D. Rodney, F. Willaime, Dislocation core reconstruction induced by carbon segregation in bcc iron, Phys. Rev. B 91 (22) (2015) 220102.
[36] G. Hachet, D. Caillard, L. Ventelon, E. Clouet, Mobility of screw dislocation in BCC tungsten at high temperature in presence of carbon, Acta Mater 222 (2022) 117440.
[37] Y.H. Li, H.B. Zhou, F. Gao, G. Lu, G.H. Lu, F. Liu, Hydrogen induced dislocation core reconstruction in bcc tungsten, Acta Mater 226 (2022) 117622.
[38] Z.Q. Wang, Y.H. Li, G.H. Lu, H.B. Zhou, Influence of carbon and oxygen on the core structure and Peierls stress of screw dislocation in molybdenum, Met 12 (3) (2022) 507.
[39] Q. Yu, L. Qi, T. Tsuru, R. Traylor, D. Rugg, J.W. Morris Jr, M. Asta, D.C. Chrzan, A. M. Minor, Origin of dramatic oxygen solute strengthening effect in titanium, Science 347 (6222) (2015) 635–639.
[40] Y. Chong, R.P. Zhang, M.S. Hooshmand, S.T. Zhao, D.C. Chrzan, M. Asta, J. W. Morris Jr, A.M. Minor, Elimination of oxygen sensitivity in α-titanium by substitutional alloying with Al, Nat. Commun. 12 (2021) 6158.
[41] Z.F. Lei, X.J. Liu, Y. Wu, H. Wang, S.H. Jiang, S.D. Wang, X.D. Hui, Y.D. Wu, B. Gault, P. Kontis, D. Raabe, L. Gu, Q.H. Zhang, H.W. Chen, H.T. Wang, J.B. Liu, K. An, Q.S. Zeng, T.G. Nieh, Z.P. Lu, Enhanced strength and ductility in a high-entropy alloy via ordered oxygen complexes, Nature 563 (7732) (2018) 546–550.
[42] P.J. Yang, Q.J. Li, T. Tsuru, S. Ogata, J.W. Zhang, H.W. Sheng, Z.W. Shan, G. Sha, W.Z. Han, J. Li, E. Ma, Mechanism of hardening and damage initiation in oxygen embrittlement of body-centred-cubic niobium, Acta Mater 168 (2019) 331–342.
[43] P.J. Yang, Q.J. Li, W.Z. Han, J. Li, E. Ma, Designing solid solution hardening to retain uniform ductility while quadrupling yield strength, Acta Mater 179 (2019) 107–118.
[44] J. Zhang, W.Z. Han, Oxygen solutes induced anomalous hardening, toughening and embrittlement in body-centered cubic vanadium, Acta Mater 196 (2020) 122–132.
[45] X.Q. Wang, Y.S. Zhang, W.Z. Han, Design of high strength and wear-resistance β-Ti alloy via oxygen-charging, Acta Mater 227 (2022) 117686.
[46] Y.H. Zhang, W.Z. Han, Mechanism of brittle-to-ductile transition in tungsten under small-punch testing, Acta Mater 220 (2021) 117332.
[47] M. Sankar, R.G. Baligidad, A.A. Gokhale, Effect of oxygen on microstructure and mechanical properties of niobium, Mater. Sci. Eng. A 569 (2013) 132–136.
[48] X.H. Min, P.F. Bai, S. Emura, X. Ji, C.Q. Cheng, B.B. Jiang, K. Tsuchiya, Effect of oxygen content on deformation mode and corrosion behavior in β-type Ti-Mo alloy, Mater. Sci. Eng. A 684 (2017) 534–541.
[49] K. Turba, R. Hurst, P. Hahner, Evaluation of the ductile-brittle transition temperature in the NESC-I material using small punch testing, Int. J. Press. Vessel. Pip. 111 (2013) 155–161.
[50] T.E. García, C. Rodríguez, F.J. Belzunce, C. Suárez, Estimation of the mechanical properties of metallic materials by means of the small punch test, J. Alloys Compd. 582 (2014) 708–717.
[51] S. Arunkumar, Overview of Small Punch Test, Met. Mater. Int. 26 (2020) 719–738.
[52] E. Altstadt, F. Bergner, M. Houska, Use of the small punch test for the estimation of ductile-to-brittle transition temperature shift of irradiated steels, Nucl. Mater. Energy 26 (2021) 100918.
[53] Y. Lu, W.Z. Han, Pre-stored edge dislocations-enabled pseudo-toughness in chromium, Acta Mater 248 (2023) 118788.
[54] V.V. Bulatov, L.L. Hsiung, M. Tang, A. Arsenlis, M.C. Bartelt, W. Cai, J.N. Florando, M. Hiratani, M. Rhee, G. Hommes, T.G. Pierce, T. Diaz de la Rubia, Dislocation multi-junctions and strain hardening, Nature 440 (2006) 1174–1178.
[55] D. Caillard, Kinetics of dislocations in pure Fe. Part I. In situ straining experiments at room temperature, Acta Mater 58 (9) (2010) 3493–3503.
[56] W.Z. Han, A. Vinogradov, C.R. Hutchinson, On the reversibility of dislocation slip during cyclic deformation of Al alloys containing shear-resistant particles, Acta Mater 59 (2011) 3720–3736.
[57] M.J. Pfeifenberger, V. Nikolic, S. Zak, A. Hohenwarter, R. Pippan, Evaluation of the intergranular crack growth resistance of ultrafine grained tungsten materials, Acta Mater 176 (2019) 330–340.
[58] D. Caillard, Kinetics of dislocations in pure Fe. Part II. In situ straining experiments at low temperature, 58(9) (2010) 3504–3515.
[59] C. Ghosh, A. Singh, J. Basu, D. Ramachandran, E. Mohandas, Microstructural and microchemical studies of phase stability in V-O solid solution, Mater. Charact. 124 (2017) 129–135.
[60] T.T. Zou, P.B. Zhang, J.J. Zhao, P.F. Zheng, J.M. Chen, First principles study of vacancy-solute complexes in vanadium, J. Alloys Compd. 763 (2018) 861–866.
[61] X.M. Zhang, Y.F. Li, Q.L. He, R.L. Li, L. Deng, L. Wang, X.L. Liu, J.F. Tang, H. Q. Deng, W.Y. Hu, Investigation of the interstitial oxygen behaviors in vanadium alloy: a first-principles study, Curr. Appl. Phys 18 (2018) 183–190.
[62] W.Z. Han, A. Vinogradovc, C.R. Hutchinson, On the reversibility of dislocation slip during cyclic deformation of Al alloys containing shear-resistant particles, Acta Mater 59 (2011) 3720–3736.
[63] X.Q. Wang, W.Z. Han, Oxygen-gradient titanium with high strength, strain hardening and toughness, Acta Mater 246 (2023) 118674.
[64] Y. Lu, Y.H. Zhang, E. Ma, W.Z. Han, Relative mobility of screw versus edge dislocations controls the ductile-to-brittle transition in metals, Proc. Natl. Acad. Sci. U. S. A. 118 (37) (2021) e2110596118.
[65] Y.H. Zhang, E. Ma, J. Sun, W.Z. Han, A unified model for ductile-to-brittle transition in body-centered cubic metals, J. Mater. Sci. Tech. 141 (2023) 193–198.